doi:10.1016/j.jmb.2006.08.059 *J. Mol. Biol.* (2006) **363**, 687–701

JMB

Available online at www.sciencedirect.com

ScienceDirect

ELSEVIER

The Structure of Apo-wild-type Cellular Retinoic Acid Binding Protein II at 1.4 Å and its Relationship to Ligand Binding and Nuclear Translocation

Soheila Vaezeslami[1], Erika Mathes[2], Chrysoula Vasileiou[1] Babak Borhan[1]* and James H. Geiger[1]*

[1]*Chemistry Department Michigan State University, East Lansing, MI 48824-1322, USA*

[2]*University of California, San Diego Department of Chemistry and Biochemistry 9500 Gilman Dr. # 037 La Jolla CA 92093-0375, USA*

**Corresponding authors*

CRABPII is a small, cytosolic protein that solubilizes and transfers retinoic acid (RA) to the nucleus while also enhancing its transcriptional activity. We have determined the first high-resolution structure of apo-wild type (WT) CRABPII at 1.35 Å. Using three different data sets collected on apo-WT CRABPII we have shown that apo- and holo-CRABPII share very similar structures. Binding of RA appears to increase the overall rigidity of the structure, although the induced structural changes are not as pronounced as previously thought. The enhanced structural rigidity may be an important determinant for the enhanced nuclear localization of the RA-bound protein. Comparison of our apo-WT with a mutant apo-CRABPII structure shows that mutation of Arg111, a conserved residue of CRABPII and a key residue in RA binding, causes structural changes in the molecule. We further investigated the structural importance of conserved residues by determining the structure of the F15W mutant CRABPII (F15W-CRABPII). Our structures also demonstrate structural changes induced by crystal packing and show that a crystal can harbor demonstrative structural differences in the asymmetric unit.

Keywords: cellular retinoic acid binding protein type II; retinoic acid; crystal structure; intracellular lipid binding proteins; retinoic acid binding proteins

Introduction

Retinoic acid (RA), a biologically active metabolite of vitamin A (retinol), acts as a morphogen during embryonic morphogenesis,[1] and is found to be indispensable for regulating vertebrate cell growth, differentiation and homeostasis.[2–5] It has also been successfully used in the treatment of acute promyelocytic leukemia (APL),[2,6,7] a variety of skin disorders, human cancers and epithelial tumorigenesis.[1,2,8–10]

Developmental gene expression can be disrupted either by an excess or deficiency of RA. Much of the biological role of RA is due to its interaction with the RA receptor (RAR), a member of the steroid/thyroid hormone receptor family of transcription factors. RAR functions as a heterodimer with the retinoid 'X' receptor (RXR) and recognizes RAR-response elements (RARE) in gene promoters in a ligand-dependant manner to regulate the transcription of these genes.[1,11–16]

RA is a hydrophobic and insoluble molecule that must be solubilized and transferred to the nucleus, where it binds to RARs. Two homologous cytosolic proteins, cellular RA binding protein type I and II (CRABPI and CRABPII),[17–19] solubilize RA, protect it from isomerization and regulate its effective concentration in the cell by either binding to excess RA and/or metabolizing RA in the cell through interaction with metabolizing enzymes.[20–26] The fact

Present address: S. Vaezeslami, Biochemistry Department, University of Wisconsin, 433 Babcock drive, Madison, WI 53706-1544, USA.

Abbreviations used: CRABPI, cellular retinoic acid binding protein type I; CRABPII, cellular retinoic acid binding protein type II; RA, retinoic acid; CRABPII•RA, CRABPII bound to RA; F15W-CRABPII, CRABPII with the F15W mutation; vdw, van der Waals; iLBP, intracellular lipid-binding protein; PDB, protein data bank; NLS, nuclear localization signal; PEG, polyethylene glycol; RAR, retinoic acid receptor; WT, wild-type.

E-mail addresses of the corresponding authors: borhan@chemistry.msu.edu; geiger@cem.msu.edu

that CRABPs are expressed in tissues that are sensitive to high concentrations of RA supports this hypothesis.[27]

CRABPs are found in virtually all vertebrates.[20] In embryos both CRABPI and II are widely expressed, although they are not co-expressed in the same cells.[28] In adult rats CRABPI is widely expressed; however, expression of CRABPII is restricted to specific tissues such as skin,[20] testis,[29,30] uterus, ovary,[31,32] choroid plexus,[33] and hematopoietic cells.[7,15]

CRABPs are small ($M_r \sim 16$ kDa), soluble proteins that belong to the family of intracellular lipid-binding proteins (iLBPs). This family is characterized by a well-defined β-barrel formed by two orthogonal five-stranded β-sheets that provide a large, deep and embedded binding cavity. Two short α-helices act as a cap to the portal of the cavity.[34]

The two isoforms of CRABP are highly homologous in human (74% identity) and among species. For example, CRABPI and II in human and mouse are 99.3% and 93.5% identical, respectively. Higher sequence identity of the same isoform (CRABPI or CRABPII) among different species as compared to different isoforms in the same species indicates these two homologues should have distinct functions, which explains the conservation of their genes during the course of evolution.[35,36] Although both CRABPs are believed to solubilize and transfer their ligands to the nucleus, experiments show that CRABPII enhances the transcriptional activity of RA,[37] while CRABPI enhances the activity of enzymes that catalyze RA degradation and therefore depresses RA efficacy in the cell.[25,26]

In 1986 Takase *et al.* demonstrated that CRABPs are carriers of RA to the nucleus and chromatin of rat testes,[38] and in 1998 Gaub *et al.* showed both CRABPI and II to be present in the nucleus.[21] In 1999, Dong *et al*. successfully showed that the rate of transfer of RA from CRABPII to RAR is highly dependent on the concentration of RAR, and the process follows a first-order kinetically controlled mechanism. This finding indicates that CRABPII directly interacts with RAR and forms a protein–protein intermediate complex to directly transfer or "channel" RA to the acceptor.[39] In the same year, Delva *et al.* showed that CRABPII, and not CRABPI, associates with the RARα–RXRα complex in a ligand-dependent manner both *in vitro* and *in vivo*, and enhanced the transcriptional activity of the RARα–RXRα heterodimer.[7] Recently, Budhu *et al.* showed that although apo-CRABPII is mostly cytosolic, upon RA binding it is localized to the nucleus. This sensitized cells to RA-induced growth inhibition and enhanced the RA-induced transcriptional activity of RARα.[36,40]

Nuclear localization is believed to occur through the recognition of a nuclear localization signal (NLS). The NLS is a short sequence of basic amino acids that regulates the transport of a protein from the cytoplasm of the cell to the nucleus. Typically deletion of an NLS sequence abrogates nuclear localization and frequently a non-nuclear protein can be localized to the nucleus by fusion to an NLS.[41,42] However, the sequence of CRABPII does not have a recognizable NLS in its primary sequence,[40] leaving the mechanism for nuclear localization undetermined.

In an attempt to understand the mechanism of CRABPII nuclear localization upon ligand binding, a comparison was made between the structures of RA-bound CRABPII (PDB ID: 1CBS) and the R111M mutant apo-CRABPII (PDB ID: 1XCA), which was the only structure of apo-CRABPII available at the time.[40,43,44] A significant conformational change was observed in the R111M CRABPII's structure, resulting in a significant change in the electrostatic potential upon RA binding. Most of this change was localized to a change in conformation of three residues, Lys20, Arg29 and Lys30 which upon RA ligation assume a three-dimensional structure that could be approximately overlaid with the structure of a classical NLS from the SV40-T antigen. In apparent confirmation of this hypothesis, mutation of all three of these residues results in a CRABPII that is less efficient in nuclear localization.[40] However, the structural conclusions were made based on the structure of a mutant of CRABPII (R111M).[43] Arg111 is a conserved residue in CRABPII (~80%),[45] and the R111M mutation results in a 45-fold decrease in the RA binding affinity of the protein.[43,46,47] Therefore, its mutation may have a significant impact on the structure of the protein. However, since attempts in crystallizing the apo-wild type (WT) had so far been unsuccessful, the apo-R111M mutant was the only apo-CRABPII crystal structure available at that time.

It has been shown that binding of the ligand to proteins in the iLBP family usually results in major changes in the structure of the protein.[34,48,49] Chen *et al*. used their structure of the R111M mutant of CRABPII to address the ligand entry issue. Comparison of the RA-bound WT CRABPII to the apo-R111M mutant CRABPII seemed to show that binding of the ligand is accompanied by major structural changes in the α2 helix, the βC–βD and the βE–βF hairpin loops of CRABPII. It was thought that these structural changes were necessary to open the binding pocket allowing RA entry. Further, a three-step mechanism of ligand entry was proposed, which consisted of: opening of the binding pocket, exposure of positive electrostatic potential that directs RA to the binding pocket, and interaction of three residues (Arg111, Arg132, and Tyr134) located deep inside the pocket, with the carboxylic group of RA to stabilize bound RA deep inside the binding cavity.[43]

To test the issues raised by Sessler *et al*.[40] and Chen *et al*.,[43] we have crystallized and determined the structure of apo-WT CRABPII at very high resolution (1.35 Å). We have also extended the resolution of the WT-CRABPII•RA complex (CRABPII•RA) to 1.48 Å resolution so that a more detailed comparison of the two structures can be made.[44] In addition, we have determined the structure of F15W-CRABPII; to

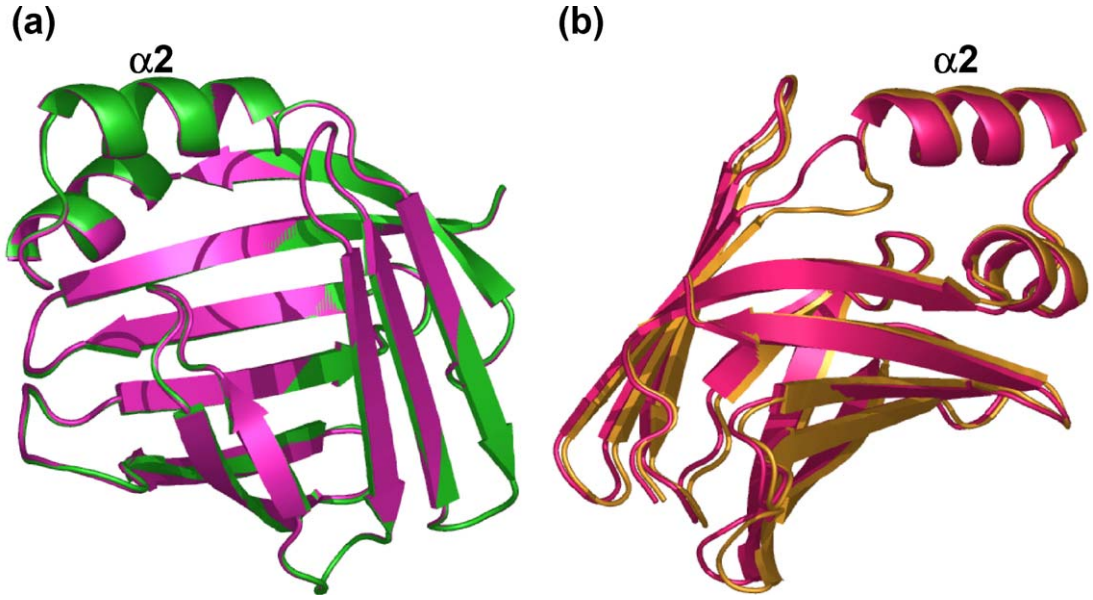

Figure 1. Structural differences between crystals of apo-CRABPII. Superimposed structures of (a) Mol A's of Xtal1 (green) and Xtal2 (purple); and (b) Mol B's of Xtal1 (hot pink) and Xtal2 (orange).

further probe the structural importance of conserved residues.

Results and Discussion

Overall structure of apo-WT CRABPII

Here we report the first crystal structure of human apo-WT CRABPII at 1.35 Å, refined to crystallographic *R*-factors of R_{work} = 14.35% and R_{free} = 20.05%. The structure is monomeric and has a *P*1 space group with two independent molecules in the asymmetric unit, identical to that of the R111M structure solved by Chen *et al.*[43] The two molecules are labeled Mol A and Mol B consistent with Chen *et al.* (Figure 1).[43] Apo-WT CRABPII, like other iLBPs, has two α helices and a β barrel. The β barrel is formed by two five-stranded β sheets that are almost orthogonal to each other and form a deep, large and embedded binding pocket. The α1-loop-α2 motif and βC–βD and βE–βF hairpin loops form the portal of the pocket. RA binds deep inside the pocket, with only its ionone ring partially solvent exposed at the portal of the pocket.[44,46]

Complete diffraction data were collected from each of three different crystals of apo-WT CRABPII, Xtal1, Xtal2 and Xtal3. Since the structures resulting from Xtal2 and Xtal3 were virtually identical, only the higher resolution data set (from Xtal2) was completely refined. Data collection and refinement statistics for Xtal1 and Xtal2 are reported in Tables 1 and 2, respectively. Analysis of Ramachandran plots is shown in Table 2 and is also discussed in Materials and Methods.

Both structures show a similar secondary structure as determined by DSSP.[50] Superposition of the

Table 1. X-ray data collection statistics

	Apo-CRABPII Xtal1	Apo-CRABPII Xtal2	F15W-CRABPII	Holo-CRABPII
Space group	*P*1	*P*1	*P*1	$P2_12_12_1$
Unit cell dimensions				
a (Å)	34.46	34.48	34.58	44.15
b (Å)	37.70	37.22	37.03	46.59
c (Å)	56.56	57.60	58.69	77.55
α (°)	72.63	73.09	102.00	90.00
β (°)	76.35	75.74	106.12	90.00
γ (°)	87.29	87.22	93.00	90.00
Wavelength (Å)	1.0000	1.0000	0.99298	1.0000
Resolution range (Å)	50.0–1.35 (1.40–1.35)	50.0–1.55 (1.61–1.55)	50.00–1.51 (1.56–1.51)	39.81–1.48 (1.53–1.48)
Average I/σ	14.56 (1.77)	23.70 (3.36)	14.38 (1.69)	28.19 (5.08)
Total reflections	512,955	196,753	356,236	50,640
Unique reflections	56,961	38,968	42,559	27,332
Completeness (%)	88.4 (56.5)	92.3 (68.1)	92.8 (75.0)	95.5 (96.4)
R_{sym} (%)	4.2 (26.1)	4.2 (15.7)	3.2 (26.1)	4.4 (13.9)

Values in parentheses refer to the last resolution shell.

Table 2. Structure refinement statistics

	Apo-CRABPII Xtal1	Apo-CRABPII Xtal2	F15W-CRABPII	Holo-CRABPII
Average *B*-Factor (Å^2)	16.78	18.82	17.96	15.99
R_{work} (%)	14.35	13.94	17.15	12.30
R_{free} (%)	20.05	19.67	24.25	17.09
Number of water molecules	386	299	455	209
Total reflections used	50,364	35,954	39,495	26,145
Total reflections in work set	45,282	32,359	35,549	23,523
Total reflections in test set	5082	3595	3946	2622
RMSD from ideality				
Bond lengths (Å)	0.020	0.019	0.016	0.019
Bond angles (°)	1.888	1.750	1.681	1.776
Ramachandran plot				
Most favored (%)	94.3	93.5	93.8	95.2
Allowed (%)	4.9	5.7	5.3	4.0
Generously allowed (%)	0.4	0.4	0.0	0.8
Disallowed (%)	0.4	0.4	0.9	0.0
PDB code	2FS6	2FS7	2FRS	2FR3

two structures (Figure 1) shows that the Mol A's are virtually identical (the overall RMSD between the Cα atoms of the Mol A's is only 0.198 Å). However, Mol B's in Xtal1 and Xtal2 show distinct differences in the loop region connecting α2 to βB (residues 36–40), while α2 has an identical conformation in both molecules (Figure 1(a) and (b)). The overall RMSD value between the Cα atoms of the Mol B's is 0.689 Å. However, most of this difference comes from the loop region (residues 36–40), as the RMSD between the Cα atoms of these residues is 3.35 Å. Excluding these residues from the RMSD calculation gives an overall RMSD value of 0.26 Å. Therefore, although these crystals were grown from an identical condition and have identical unit cells and crystal packing, there is a substantial difference in conformation between two crystallographically identical molecules.

Comparison between Mol A and Mol B of apo-WT CRABPII

We refer to Xtal1 when comparing the two molecules in the asymmetric unit, because it has higher resolution and better data statistics. The two molecules have very similar structures except for structural changes in α2, the loop connecting α2 to βB, and the βC–βD hairpin loop. There are also minor differences in the βF–βG and βI–βJ hairpin loops (Figure 2). The overall RMSD value between the Cα atoms of Mol A and Mol B is 0.92 Å. The differences become noticeable at Lys20, located at the C terminus of α1 (*xyz* deviation of 0.920 Å), and increase moving toward the C terminus of α2 and the loop connecting α2 to βB. Ser37, in the middle of the loop, has a maximum *xyz* deviation (3.384 Å) between equivalent Cα positions in Mol A and Mol B. The differences decrease at the N terminus of βB. If residues 20 to 40 (the loop-α2-loop region) are excluded from the RMSD calculation between the two molecules, the overall RMSD value falls to 0.73 Å. The RMSD values for residues 20 to 40 is equal to 1.60 Å. As shown in Figure 2, in Mol B the C terminus of α2 moves toward the binding site of RA, and away from α1 (maximum *xyz* deviation between the Cα atoms of the α2 in Mol A and Mol B is equal to 2.953 Å at Ala35, the last residue of α2). Since residues on the βC–βD hairpin loop directly interact with the residues on the third helical turn of α2, the βC–βD hairpin loop moves concurrently with the movement of the α2 helix and away from the binding cavity. This movement of the hairpin loop causes the C terminus of βC and the N terminus of βD to move away from the binding cavity as well. The second helical turn of α1 shows some minor movement compared to Mol A. The maximum *xyz* deviation between the Cα atoms of α1 in Mol A and Mol B is equal to 1.247 Å at Leu21, the last residue of α1.

The dissimilarities between the two molecules indicate regions of flexibility and must be due to different crystal packing environments for the two molecules. As assessed by the program CONTACT in the CCP4 suite,[51] the α2 helix in Mol A is involved in three hydrogen bond and 16 van der Waals (vdw) contacts with neighboring molecules, while that of Mol B is involved in four hydrogen bonds and 59 vdw contacts. All three hydrogen bonds of Mol A involve interactions of the guanidino group of Arg29, located on the second helical turn of α2, with the carbonyl group and side-chain of Glu137 of a symmetry related molecule. In Mol B there are two hydrogen bonds between the guanidino group of Arg29 and the carboxylate group of Glu137 of a symmetry related molecule; however, there are two additional hydrogen bonds between α2 and neighboring molecules. One is between the carbonyl group of Lys30, located on the second helical turn of α2, with the side-chain of Thr131 of a symmetry related molecule; and the other is between the carbonyl group of Ala34, on the third helical turn of α2, and the side-chain of Asn14 of a symmetry related molecule. The additional hydrogen bonds and vdw contacts between the second and third helical turns of α2 in Mol B with neighboring molecules drag the helix toward the βC–βD hairpin loop. The βC–βD hairpin loop moves concurrently with the movement of the helix. Therefore direct crystal-packing interactions can explain differences in the structures of Mol A and Mol B in the asymmetric unit.

In Mol A but not in Mol B, the guanidino group of Arg111 indirectly interacts with α2 and the loop connecting α2 to βB through two solvent-mediated interactions. The paths of these two interactions

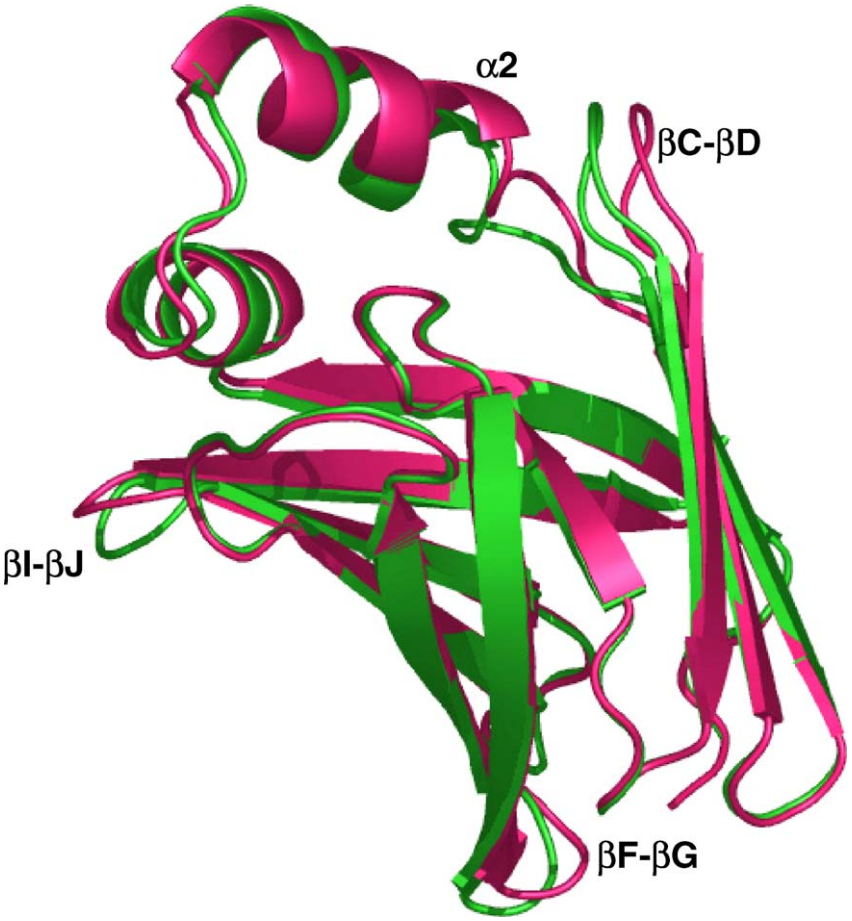

Figure 2. Structural differences between the two molecules in the asymmetric unit of apo-CRABPII. Superimposed structures of Mol A (green) and Mol B (hot pink) of Xtal1.

are shown in Figure 3 and are: (1) guanidine group of Arg111→water 204→carboxylate of acetate 4→guanidino group of Arg132→carbonyl of Ala36; and (2) guanidino group of Arg111→water 204→carboxylate of acetate 4→guanidino group of Arg132→water 33→carbonyl of Val33. Val33 is located on the third helical turn of α2 and Ala36 is on the loop connecting α2 to βB. Acetate is one of the crystallization reagents and binds in the cavity by occupying the position of the carboxylate group of RA. The same solvent-mediated interaction exists in Mol A of Xtal2, but a chloride ion occupies the position of acetate in Xtal1, confirming that the contact does not rely on acetate. Xtal3 has an acetate molecule exactly as observed in Xtal1.

Arg111 has exactly the same conformation in Mol A and Mol B. However, Arg132 has distinct conformations in each molecule. In Mol A it faces the α2 helix and makes hydrogen bonds with Val33 and Ala36, while in Mol B it looks away from the loop and binds to the carbonyl group of Val76, on the βC–βD hairpin loop, and the oxygen of Ser12, the last residue of βA through other water networks.

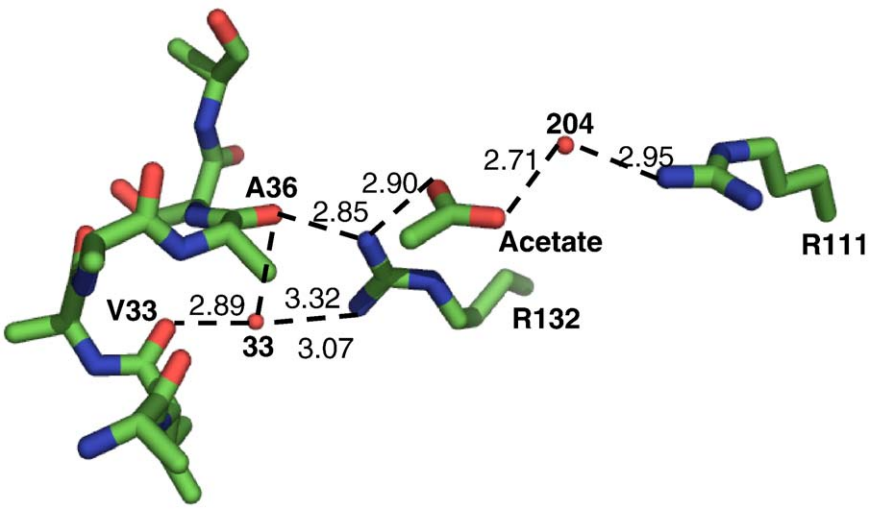

Figure 3. Solvent-mediated interaction between Arg111, Val33 and Ala36 in Mol A of Xtal1.

Also in Xtal2 and Xtal3, and not in Xtal1, the Nε nitrogen of Arg132 binds to the main-chain nitrogen of Lys38 through a solvent molecule (water or chloride). In Xtal1 the loop connecting α2 to βB has a different conformation compared to that in Xtal2 and Xtal3 and therefore is positioned further away from Arg132 (Figure 1(b)). Thus, in Mol B of Xtal1 there is no interaction between Arg132 and Lys38. This observation indicates that since in Mol A Arg132 faces the loop and makes a direct and tight hydrogen bond with Ala36, it fixes the position of the α2 helix and the loop in this molecule. However, in Mol B it cannot make such a tight hydrogen bond with the loop and therefore the loop becomes flexible. The conformations of the residues mentioned above are identical in Xtal1, Xtal2 and Xtal3 (data not shown for Xtal3).

But why does Arg132 have two different conformations in the two molecules? Different intermolecular interactions of the C terminus of α2 in Mol B as compared to that of Mol A eliminates the interactions of Arg132 with Ala33 and Val36 inside the pocket and therefore Arg132 assumes a different conformation to make a hydrogen bond to Val76 and Ser12 through different water-mediated interactions.

Changes induced upon R111M mutation

Arg111 is not only a highly conserved residue,[45] it is also one of the key RA-binding residues,[43] and therefore mutation of this residue could potentially cause major changes in structure.

Comparing Mol A of apo-WT to that of the R111M structure shows that the α2 helix and βC–βD hairpin loop are strikingly different in the R111M structure (Figure 4(a)). However, the α2 helices have identical conformations in Mol B of the two structures (Figure 4(b)). The major difference between Mol B of apo-WT and R111M lies in the βC–βD, βG–βH, and βI–βJ hairpin loops. The loop connecting α2 to βB, residues 36 to 39, has a very similar conformation in Mol B of Xtal1 and the R111M structure (Figure 4(b)).

It was reported by Chen *et al.*[43] that α2 of Mol A in R111M is not involved in intermolecular hydrogen bond interactions resulting from crystal packing and makes only eight intermolecular crystal packing vdw contacts, while that of Mol B is involved in seven hydrogen bonds and 43 vdw contacts. Therefore, it was suggested that structural differences between Mol A and Mol B of R111M were due to the fact that the structure of Mol B is an artifact of crystal-packing while that of Mol A is the actual conformation of apo-CRABPII. However, α2 of Mol A and Mol B of apo-WT CRABPII are both involved in crystal packing hydrogen bonds and vdw contacts. α2 of Mol A is involved in three hydrogen bonds and 16 vdw contacts and that of Mol B is involved in four hydrogen bonds and 59 vdw contacts.

As discussed here, in Xtal1 Arg111 interacts with carbonyl groups of Val33 and Ala36 through two short solvent-mediated interactions (Figure 3). These residues are located on the α2 helix and the loop connecting this helix to βB, respectively. The network interaction keeps these regions tight at their place. Therefore, it is expected that mutation of Arg111 could allow the helix and loop to be mobile, and therefore cause major structural changes. Investigating the interactions inside the pocket of the R111M mutant shows that there is no interaction between Met111 and residues on the helix or the loop, which indicates that movement of the α2 helix of Mol A of R111M as compared to that of apo-WT must be due to mutation of this key residue. Also Arg132 has a distinct conformation in this structure from that in Mol A of apo-WT and has no hydrogen bond interaction with the helix or the loop.

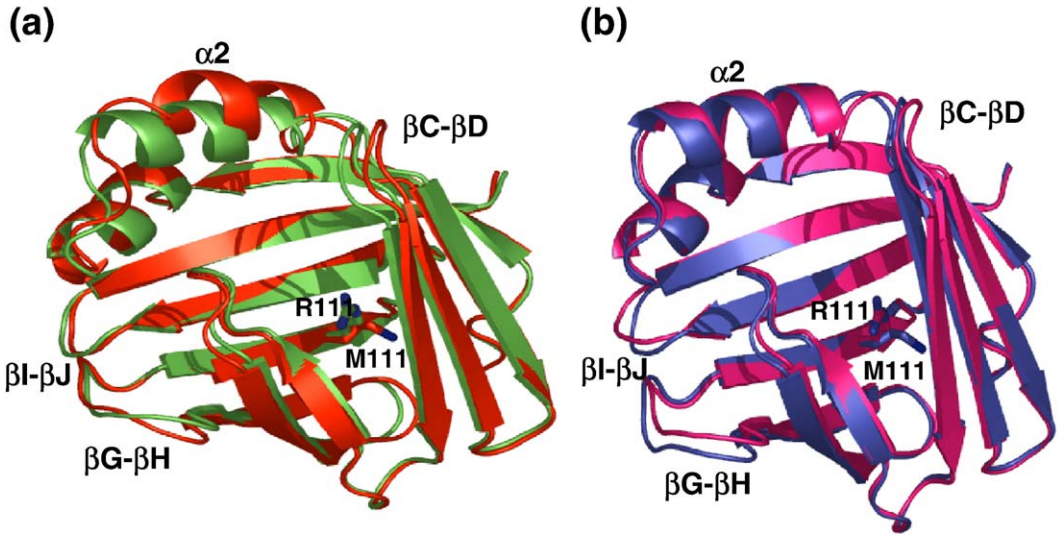

Figure 4. The significant structural consequences of the R111M mutation. (a) Mol A's of R111M (red) and Xtal1 (green); and (b) Mol B's of R111M (blue) and Xtal1 (hot pink) are superimposed.

Chen *et al.*[43] studied the conformational differences between apo-R111M and CRABPII•RA and suggested a three-step mechanism of ligand entry into CRABPII. This mechanism involved first portal opening involving unwinding of the α2 helix and motion of the βC–βD and βE–βF hairpin loops, where unwinding of the α2 helix was thought to be essential for RA entry. Three positively charged residues, Arg29, Arg59 and Arg132, were then thought to "direct" the RA carboxylate group into the binding cavity. These residues would then flip out of the binding cavity in the last binding step. Our structure of apo-WT CRABPII, however, is not consistent with this hypothesis because we do not see the same conformational changes between the apo and bound CRABPII. First, the α2 helix in apo-WT CRABPII and the CRABPII•RA complex is identical in most of our structures, in contrast to the large conformational change seen in the R111M structure. Furthermore, both Arg29 and Arg132 have identical conformations in the bound and apo forms of the protein, indicating that conformational change of these residues is not required to direct RA binding. We conclude that in fact the most significant conformational differences between the apo-R111M structure and the WT-CRABPII•RA complex structure are due to the mutation of the very conserved Arg111 residue. Arg59, the first residue of βD, located at the portal of the pocket, has the same conformation in Xtal1 and Xtal2 but is different from CRABPII•RA and R111M. In both apo-WT and CRABPII•RA, the side-chain of Arg59 is located toward the exterior of the pocket; however, in CRABPII•RA it is forced away from the portal of the pocket to provide enough space for the dimethyl group of the ionone ring. In contrast, in the R111M structure, the conformation of Arg59 is strikingly different and unlike other structures it bends toward the interior of the pocket and has a water network interaction with Arg132. Therefore, we believe that the three-step mechanism of RA entry proposed by Chen *et al.*,[43] based on comparing the structure of apo-R111M and holo-CRABPII is not consistent with the structures of apo-WT CRABPII we have determined.

Changes induced upon F15W mutation on the apo-WT structure

To better understand the importance of conserved residues for the structural integrity of the iLBP fold, we decided to determine the structure of another CRABPII mutant. Among all 52 members of iLBPs Phe15, the first residue of the α1 helix, is a fully conserved residue (100%). Therefore, we decided to conservatively mutate this fully conserved residue to Trp and study the impact of this mutation on the structure. F15W-CRABPII was crystallized and the structure was determined at 1.51 Å at crystallographic *R*-factors of R_{work} = 17.15% and R_{free} = 24.25%. Similar to apo-WT and apo-R111M structures, the crystals were in the *P*1 space group with two molecules in the asymmetric unit. The data collection and refinement statistics are reported in Tables 1 and 2, respectively. Interestingly we observed that the α2 helix of Mol A is completely disrupted in F15W-CRABPII mutant structure (Figure 5(a)). Though α2 in Mol B is well defined, this helix and the loop connecting α2 to βB have a different conformation from that in Mol B of apo-WT and R111M (Figure 5(b)). In fact Mol B of this mutant has a very similar conformation to that of Mol A of apo-WT. Therefore, this structure provides further confirmation for the high mobility of this loop in CRABPII and also gives further evidence that mutations of

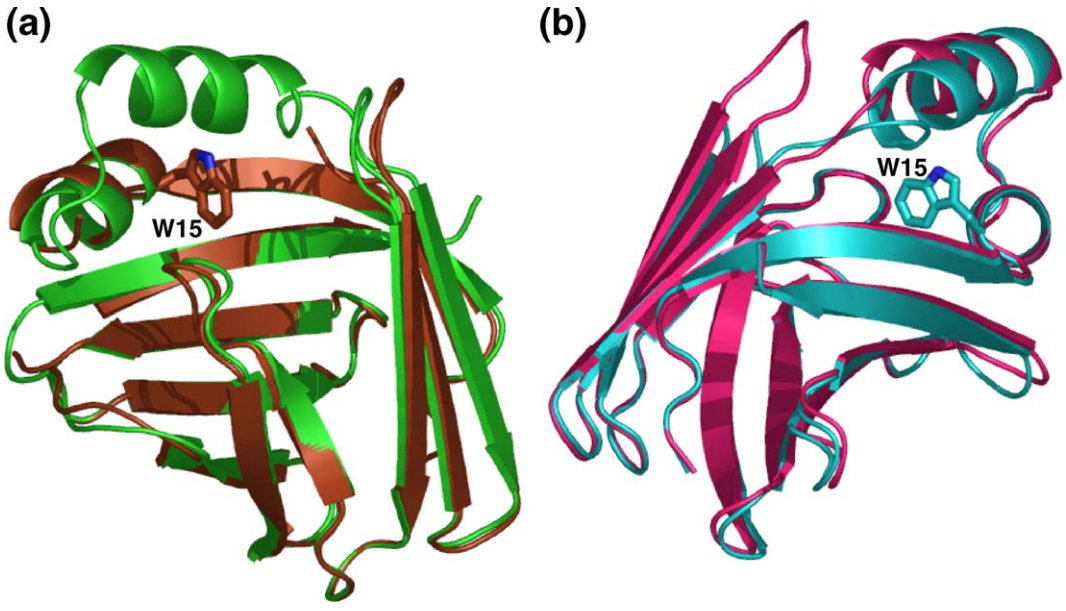

Figure 5. The F15W mutation results in significant structural change. (a) Mol A's of F15W-CRABPII (brown) and Xtal1 (green); and (b) Mol B's of F15W-CRABPII (cyan) and Xtal1 (hot pink) are superimposed.

conserved residues in the iLBP fold can result in significant structural variance. This mutant is still capable of RA binding, though the affinity is significantly reduced (K_d = 40(±4) nM) compared to WT-CRABPII (K_d = 2.0(±1.2) nM).[52]

Overall structure of CRABPII•RA and comparison with apo-WT CRABPII

We have also re-determined and refined the structure of CRABPII•RA to an improved resolution of 1.48 Å with very good crystallographic *R*-factors of 12.30% and 17.09% for R_{work} and R_{free}, respectively. The data collection and refinement statistics are reported in Tables 1 and 2, respectively.

The CRABPII•RA complex was previously crystallized in a different crystallization condition and the structure refined at 1.80 Å by Kleywegt *et al.* (PDB ID: 1CBS).[44] Our structure is identical to the previously published structure of CRABPII•RA, with the same space group ($P2_12_12_1$) and similar cell constants. RA binds deep inside the binding pocket and the carboxylic group of RA interacts with Arg111, Arg132, and Tyr134. Only the β ionone ring is partially solvent exposed at one of its edges.[46]

As mentioned earlier, Chen *et al.* believed that Mol A of apo-R111M shows the actual structure of apo-CRABPII and therefore chose Mol A over Mol B for comparing apo- and holo-CRABPII. Superimposition of Mol A of apo-R111M on CRABPII•RA showed that there were significant structural differences between the two molecules in the α2 helix, βC–βD and βE–βF hairpin loops, which were thought to be necessary for opening the binding pocket and making RA-entry possible (see Figure 3 of Chen *et al.*[43]).

We compared the structures of both molecules of apo-CRABPII to that of CRABPII•RA to evaluate these hypotheses. Comparing Mol A and CRABPII•RA (Figure 6(a)) shows that in fact these two structures are almost identical (RMSD = 0.500) except in the βC–βD hairpin loop region. In the apo structure Arg59 on this hairpin loop, has a water-mediated interaction with the carbonyl group of Ala32, which keeps Arg59 close to the portal of the pocket and in the path of RA entry. However, in

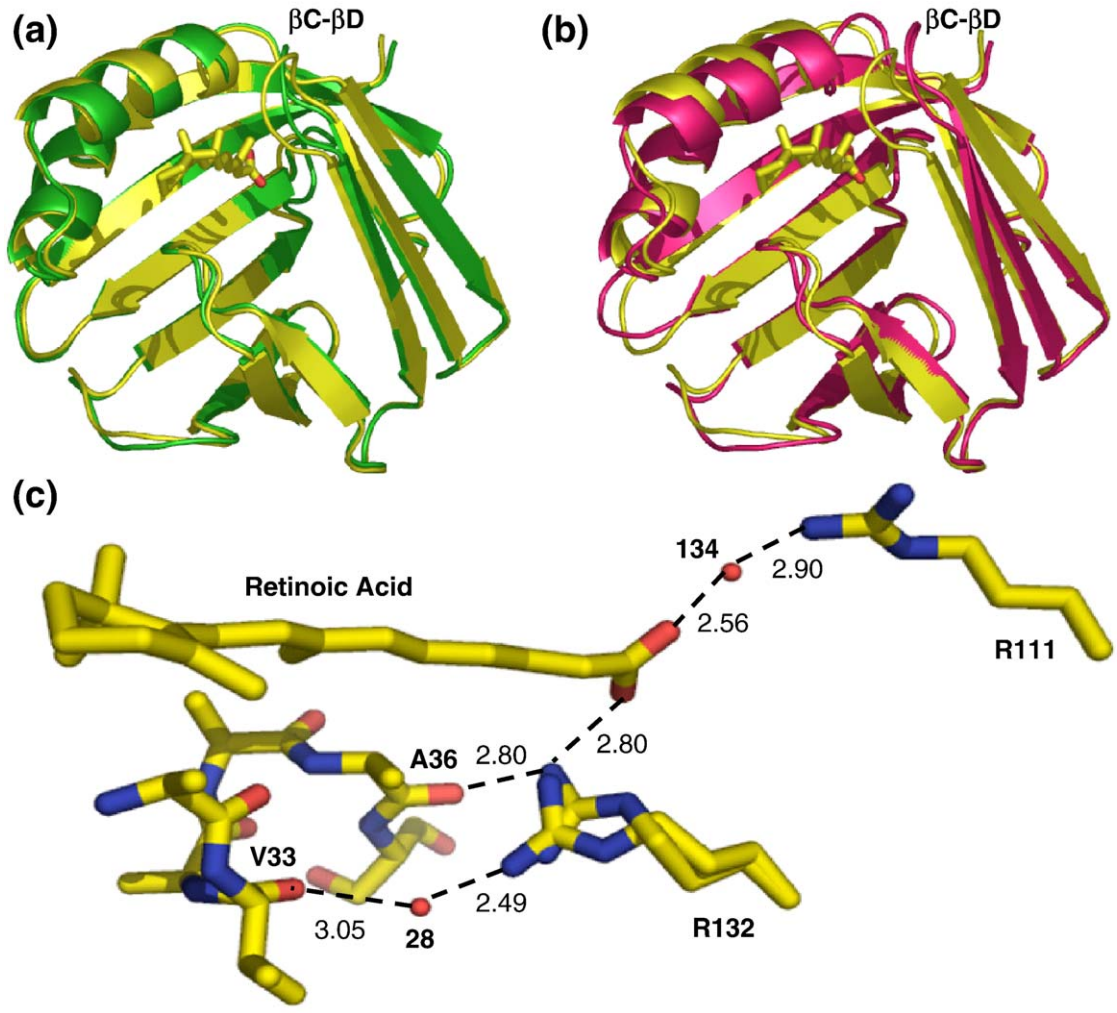

Figure 6. Structural changes to apo-CRABPII that arise upon RA binding. (a) Mol A (green), and (b) Mol B (hot pink) of Xtal1 and CRABPII•RA (yellow). (c) The water-mediated interaction between Arg111, Ala36 and Val33 that stabilizes the α2 helix.

the holo structure RA pushes the mediating water molecules away and Arg59 moves away from the portal to give RA space to enter the pocket. Also Val58 on the βC–βD hairpin loop moves closer to the binding pocket to form vdw contacts with C19 of RA. It should be mentioned that the same interactions were observed in the published structure of CRABPII•RA (PDB ID: 1CBS).

Although the βC–βD hairpin loop shows some minor differences, they are not as significant as what had been observed when the structures of apo-R111M and CRABPII•RA were compared. Chen *et al*.[43] had suggested that this hairpin loop opens in apo-CRABPII to allow RA entry and then closes when RA enters the pocket, while apo-WT-CRABPII does not show such a movement for the hairpin loop. The α2 helix has an identical conformation in both structures, which indicates that this helix does not change its conformation upon ligation contrary to the R111M structure. So the major differences observed when comparing the structures of apo-R111M and CRABPII•RA were actually the result of the R111M mutation, not RA binding.

Comparing the structure of Mol B and CRABPII•RA (Figure 6(b)) shows that the C terminus of the α2 helix and the loop connecting α2 to βB are significantly different in the two structures. As explained above the crystal packing environment of Mol B results in the altered conformation of this region and we therefore believe that its altered conformation is an artifact of crystal packing. The conformation of the α2 helix in Mol B does not leave enough space for RA to enter and bind inside the pocket: the second helical turn of the helix is very close to where RA binds inside the pocket and its residues would collide with RA. Also Arg132 has a different conformation in Mol B than in Mol A and is also in the way of RA entry. Therefore, we believe that Mol A shows the "real" conformation of apo-WT CRABPII (or at least the closest that we can get to "real" from a crystal structure) and is compatible with RA entry.

Here using three independent sets of diffraction data, collected on three different crystals of apo-WT we demonstrated that apo-WT has an almost identical structure to CRABPII•RA with only minor differences in the βC–βD hairpin loop. This hairpin loop is at the portal of the binding cavity and tends to close up the opening of the pocket upon RA ligation (Figure 6(a)).

It is interesting to note that very similar structures of these molecules, especially in the α2-helix and loop region correlate with the very similar solvent-mediated interactions in the binding cavity of both CRABPII•RA and apo-WT Mol A. This occurs because an acetate (Xtal1) or a chloride (Xtal2) ion replaces the carboxylate group of RA in the Mol A of apo-WT structure. This carboxylate or chloride serves to bridge Arg111 to the opposite side of the binding cavity, stabilizing this region. Both acetate and RA bind inside the cavity and form tight hydrogen bonds with Arg132 and Tyr134 (Figure 3 and Figure 6(c)). The network starts at Arg111 and ends at Val33 and Ala36, located on the α2 helix and the loop region (similar to the network in Mol A of apo-WT). The path of the network, shown in Figure 6(c), is: (1) guanidino group of Arg111→water 134→carboxylate of RA→guanidino group of Arg132→carbonyl of Ala36; and (2) guanidino group of Arg111→water 134→carboxylate of RA→guanidino group of Arg132→water 28→carbonyl of Val33. In contrast, this water-mediated interaction is lost in Mol B of apo-WT due to crystal packing. The differences in Mol A and Mol B of the apo structures emphasize the increased flexibility of apo-CRABPII over holo-CRABPII.

Comparison between the crystal and NMR structures

The solution structures of apo-WT (PDB ID: 1BLR) and the R111M mutant (PDB ID: 1BM5) of CRABPII both have been determined by Wang *et al*.[46,53] We have compared these two structures with the previously published crystal structure of CRABPII•RA, and showed that the structure of R111M is more similar to holo-CRABPII than apo-CRABPII in both structural and dynamic properties.[46] We compared these two solution structures to our crystal structure of apo-WT CRABPII. This comparison has shown that the NMR structure of the R111M mutant (PDB ID: 1BM5) is similar (with high RMSD of 3.56 Å) to that of apo-WT, which itself is identical to holo-CRABPII. However, the NMR solution of apo-WT CRABPII (PDB ID: 1BLR) is dramatically different from our crystal structure of this protein. The α1-loop-α2 region and the βC–βD, βE–βF and βG–βH loops have significantly different conformations in this structure. Particularly α2 is completely unwound and has opened up toward the exterior of the pocket.[50] These changes were thought to be necessary for opening of the pocket and ligand entry. However, we believe that since the ionone ring of RA is exposed at the portal, the ligand seems to find its way toward the interior of the pocket without requiring significant structural differences between the apo- and holo-CRABPII. In other words we believe that loosing the integrity of the structure, as observed in the NMR structure of apo-WT, should not be necessary for RA entry. Our three different crystal structures of apo-WT show that the apo- and holo-CRABPII are very similar and that the portal of the pocket is large enough to let RA enter the pocket without causing dramatic structural changes. In light of both the NMR structure of apo-R111M and of our numerous structures of apo-WT CRABPII, the NMR structure of the apo-WT protein is puzzling. In fact the structures of apo-CRABPI (PDB ID: 1CBI),[54] apo-M-FABP (PDB ID: 1FTP),[55] apo-IFABP (PDB IDs: 1IFB and 1IFC),[56,57] apo-CRBPII (PDB ID: 1OPA)[48] and apo-ALBP (PDB IDs: 1ALB and 1LIB),[49,58] the only other members of the iLBPs protein family with known structures, are also quite similar to our apo-CRABPII crystal structure and none display the extreme structural changes seen in the apo-CRABPII NMR-determined structure.

Comparison between the crystal structures of apo-CRABPI and apo-CRABPII

Our apo-CRABPII is monomeric while apo-CRABPI, unlike other iLBPs forms a dimer. In apo-CRABPI five new hydrogen bonds are formed between the βD strands of Mol A and Mol B, creating an intermolecular β-sheet between the two molecules. The movement of the βC–βD hairpin loop of Mol A towards the exterior of the pocket was believed to be essential for the formation of the intermolecular β-sheet resulting in dimerization. Further, it was suggested that formation of this 20 stranded double β-barrel is essential for opening the portal of the pocket and may be the ligand entry mechanism in CRABPI.[54] Our crystal structure of apo-WT CRABPII is very similar to the structure of apo-CRABPI except that it does not dimerize.

The nuclear localization signal in CRABPII•RA

Although CRABPII is a cytosolic protein, upon binding to RA it translocates into the nucleus to transfer RA to the nuclear receptor RAR.[36] However, CRABPII does not have a recognizable NLS in its primary structure, leaving open the question of how CRABPII is recognized by adaptor proteins (α importins) and why holo-CRABPII is far more efficiently localized in the nucleus relative to apo-CRABPII. Sessler *et al.*[40] observed structural differences between Mol A of apo-R111M and holo-CRABPII and calculated electrostatic surface potentials of these two proteins.[40] This showed that CRABPII•RA has a positively charged patch on the two α helices that is not present in apo-R111M (see Figure 3(b) of Sessler *et al.*[40]). Three basic residues, Lys20 (on the second helical turn of the α1), Arg29 and Lys30 (both on the second helical turn of α2) make up this positive patch (Figure 7). These residues assume different conformations in holo-CRABPII *versus* apo-R111M that lead to a positive electrostatic surface potential on holo-CRABPII and a neutral surface potential on apo-R111M. Comparison of the two structures by Sessler *et al.*[40] showed that upon RA binding these three residues assume an NLS-like structure, similar to what is observed in a classical NLS, SV40-T antigen. They showed that three SV40 peptide residues (Lys128, Lys129 and Lys131) could be approximately superimposed on the three basic residues in CRABPII•RA (Figure 3(g) of Sessler *et al.*[40]), though the superposition was far from perfect. However, comparing the conformations of these residues in apo-WT with CRABPII•RA (our data) shows that Lys20, Arg29 and Lys30 have very similar conformations in apo- and holo-CRABPII (Figure 7(a)). As shown in Figure 7(b), Arg29 and Lys20 have very similar conformations in both CRABPII•RA structures (our data *versus* 1CBS). Though the side-chain of Lys30 has a different orientation between our structure and 1CBS, it is solvent-exposed in both, and has a higher than average *B* factor in both structures, indicating significant side-chain flexibility. Considering the fact that these residues are long and located at the surface of the molecules, side-chain conformational differences and high *B*-factors in the different structures are not unexpected. Interestingly Lys20, Arg29 and Lys30 are well defined and have exactly the same conformation in Xtal1, Xtal2 and Xtal3.

In short, the differences observed in the conformation of these three basic residues by Sessler *et al.*[40] were due to structural differences that are induced by the R111M mutation. As shown in Figure 7(a), movement of the α2 helix in Mol A of the R111M structure causes dramatic conformational change in both Arg29 and Lys30. Consistent with these observations, partial nuclear localization of apo-CRABPII is evident in the experiments performed by Sessler *et al.*[40] It is clear that RA binding rigidifies the molecule, particularly in this

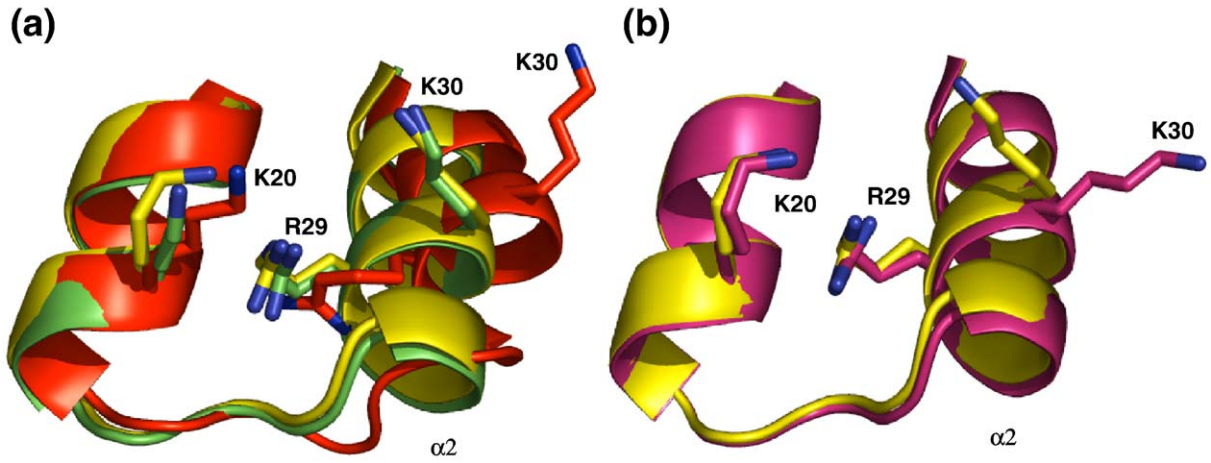

Figure 7. Significant structural change upon RA binding is not evident for the three residues identified as important for nuclear translocation. (a) Lys20, Arg29, and Lys30 in Mol A of Xtal1 (green), CRABPII•RA (yellow) and R111M (red) are superimposed. (b) Lys20, Arg29, and Lys30 in CRABPII•RA (our data, yellow) and CRABPII•RA (1CBS, magenta) are superimposed.

region, perhaps decreasing the entropic barrier to importin binding and improving the efficiency of the translocation.

Conclusion

We have determined the first high-resolution structure of apo-CRABPII. Using three different data sets collected on apo-WT CRABPII we have shown that apo- and holo-CRABPII have very similar structures and that the apo-structure is capable of increased flexibility in several regions. Comparison of our apo-WT with the apo-R111M structure shows that mutation of Arg111, one of the conserved residues of CRABPII and a key residue in binding RA to the protein, causes major structural changes in the molecule that had previously been attributed to ligand binding. Our structures demonstrate that ligand binding leads to much less pronounced structural changes than previously thought, but does lead to overall increased rigidity of the structure. This decrease in flexibility may be an important determinant in the increased nuclear localization efficiency of the RA-bound protein. In addition our structures have demonstrated structural changes induced by crystal packing in the molecule and have also shown that two apparently identical crystals can harbor demonstrative structural differences in the asymmetric unit.

Materials and Methods

Protein preparation

F15W-CRABPII

For the preparation of F15W-CRABPII site-directed mutagenesis was performed using the CRABPII-pET17b plasmid following Stratagene's Quikchange® protocol. The primers used for the mutation were: forward: 5′-CGATCGGAAAACTGGGAGGAATTGCTC-3′, reverse: 3′-GAGCAATTCCTCCCAGTTTTCCGATCG-5′. The PCR products were transfected into JM109 competent *Escherichia coli* cells for plasmid maintenance.[52]

General procedure for expression and purification of CRABPII clones

Human recombinant CRABPII was expressed and purified as described.[47] The target gene (CRABPII/pET-17b), as isolated from JM109 using Qiagen's Maxi Prep® DNA isolation kit, was transformed into *E. coli* strain BL21 (DE3)pLysS cells (Stratagene), according to standard protocols. The transformed cells were grown at 37 °C in an LB agar plate containing both ampicillin (100 μg ml^{-1}) and chloramphenicol (25 μg ml^{-1}). A single colony was inoculated in 100 ml of LB containing the same amount of the two antibiotics and grown overnight with shaking at 250 rpm at 37 °C. This culture was then transferred to 1 l of LB with the same antibiotics. The culture was incubated at 37 °C until A_{600} reached between 0.6 to 0.8. The expression was induced by addition of 0.4 mM isopropyl-1-thio-β-D-galactopyranoside (IPTG). The growth was continued for another 4 to 5 h at 30 °C. The cells were harvested by centrifugation (6000 rpm, 30 min) and frozen at −80 °C. The frozen cells obtained from a 2 l growth were thawed on ice and resuspended in 100 ml of 10 mM Tris–HCl (pH 8.0). The suspended cells were lysed by five 45 s bursts of sonication (probe sonicator, Biologics Inc., 60% power) on ice and centrifuged for 15 min at 4 °C at 5000 rpm. The supernatant was subjected to FastQ (Q-sepharose Fast Flow Resin) column chromatography (80 ml of bed volume; Amersham Biosciences), which was pre-equilibrated with 10 mM Tris–HCl (pH 8.0) buffer. The column was washed using the same buffer and proteins were eluted using NaCl gradient of 0 to 200 mM. CRABPII was eluted in 100 mM–150 mM NaCl. The fractions were analyzed by SDS–20% (w/v)polyacrylamide gel electrophoresis and those of the highest purity (~95%) were pooled together and desalted using a Vivaspin concentrator (Vivascience) with a 5000 M_r cutoff (10,000 M_r cutoff concentrators showed some protein leakage through the membrane). The desalted protein solution was further purified on a BioRad system (BioLogics Duo Flow, BioRad) using a Source15Q column (Amersham Biosciences) anion exchange column. Fractions were located by measuring the A_{280} of the fractions and analyzed by SDS–20% PAGE. All the steps of purification were performed at 4 °C. The most pure fractions (~95%) were pooled together, concentrated and buffer exchanged (100 mM Tris–HCl (pH 8.0)) in Vivaspin (Vivascience) concentrators to a concentration of ~16-20 mg ml^{-1}, determined by measuring the A_{280}. The pure, concentrated protein solution was aliquoted into 100 μl fractions and stored at −80 °C.

Preparation of the CRABPII•RA complex

All-*trans*-RA was purchased from Sigma. The complex of CRABPII with all-*trans*-RA was prepared fresh, before each crystallization experiment. The preparation was performed essentially as described.[59] Since RA is light sensitive, all the manipulations of holo-CRABPII were performed in the dark or under red light. We found that crystals of apo-WT cannot tolerate more than ~10% ethanol. Therefore, a saturated RA solution in ethanol was made to keep the percentage of ethanol below 10%, while adding ~ ten equivalents of the ligand. The protein solution was diluted almost ten times with 100 mM Tris–HCl (pH 8.0) buffer to a concentration of ~1.5 mg ml^{-1}. Ten equivalents of RA were added and the solution was re-concentrated to ~15 mg ml^{-1}, using Vivaspin concentrators. The CRABPII•RA complex was stored in lightproof tubes at 4 °C for crystallization later.

Crystallization and data collection

Apo-WT CRABPII

Apo-WT CRABPII crystals were grown by hanging drop vapor diffusion at room temperature (25 °C). Two μl of the purified protein solution (at a concentration of 16–20 mg ml^{-1} in 100 mM Tris–HCl (pH 8.0) was mixed with an equal volume of the reservoir solution. The best crystals appeared using reservoir solutions containing either one of the following solutions: (1) 0.2 M sodium acetate, 0.1 M Tris–HCl (pH 8.0) (or pH 8.5), 30% (w/v) PEG 4000 (or 8000), which is identical to reagent 22 of crystal screen 1 (Hampton Research); or (2) 0.1 M bis- Tris– propane (pH 6.5), 30% PEG 4000. Crystals appeared in three days and reached their maximum dimensions (0.03 mm × 0.05 mm ×

0.05 mm) in a week. Crystals were stabilized by quick soaking in a cryo-protectant solution consisting of the reservoir solution and 30% (v/v) glycerol as the cryo-protectant. Crystals were mounted in nylon loops (Hampton Research) and flash-frozen using liquid nitrogen. Diffraction data were collected at the BioCars beamline (section 14-ID-B) of the Advanced Photon Source (APS) synchrotron facility (Argonne, IL) using a MAR-CCD (165 mm) detector, a wavelength of 1.0000 Å and under a stream of nitrogen gas at ~−160 °C. The crystal-to-detector distance was 100 mm and 200 1° oscillation images were collected. Crystals obtained from 0.2 M sodium acetate, 0.1 M Tris–HCl (pH 8.0), 30% PEG 8000 were the best diffracting crystals (1.35 Å) although the other crystals also diffracted to high resolutions of 1.5–1.6 Å.

Our initial attempts at crystallizing apo-WT CRABPII used protein with an N-terminal His_6-tag and resulted only in poorly diffracting crystals. Thus, removal of the His-tag was critical to produce well-diffracting crystals in this case.

F15W-CRABPII

The F15W CRABPII was crystallized as described for apo-WT CRABPII. Crystals were grown at 0.2 M bis- Tris–propane (pH 6.5) and 30% PEG 4000, which is identical to one of the apo-CRABPII crystallization conditions. Crystals appeared after three days and reached their maximum size (0.1 mm × 0.2 mm × 0.2 mm) after about seven days. Data were collected at the SBC beamline at the APS synchrotron facility. A total of 239 1° oscillation images were collected at a wavelength of 0.99298 Å.

CRABPII•RA

Crystallization was performed following the apo-CRABPII crystallization procedure; however, since RA is light sensitive all manipulations of CRABPII•RA were performed in the dark or under red light. Crystallization boxes were covered with aluminum foil to avoid exposure to light. The best crystals were obtained using a reservoir solution containing 30% PEG 4000, 0.1 M sodium citrate/citric acid (pH 5.4), and 0.2 ammonium acetate, which is similar to that described.[44] Tetragonal shape crystals were obtained in less than a week and reached their maximum size in two weeks. Crystals were cryo-protected in the dark in a solution identical to the reservoir solution plus 30% glycerol. Diffraction data were collected at the COM-CAT beamline (32-ID) of APS synchrotron facility in room light, as frozen crystals are stable to light for long periods of time.

Two data sets were collected, one with minimal exposure to avoid intensity overload of the low resolution reflections, and one with longer exposure times to better measure the weaker high resolution reflections. Data sets were integrated using DENZO and scaled and merged

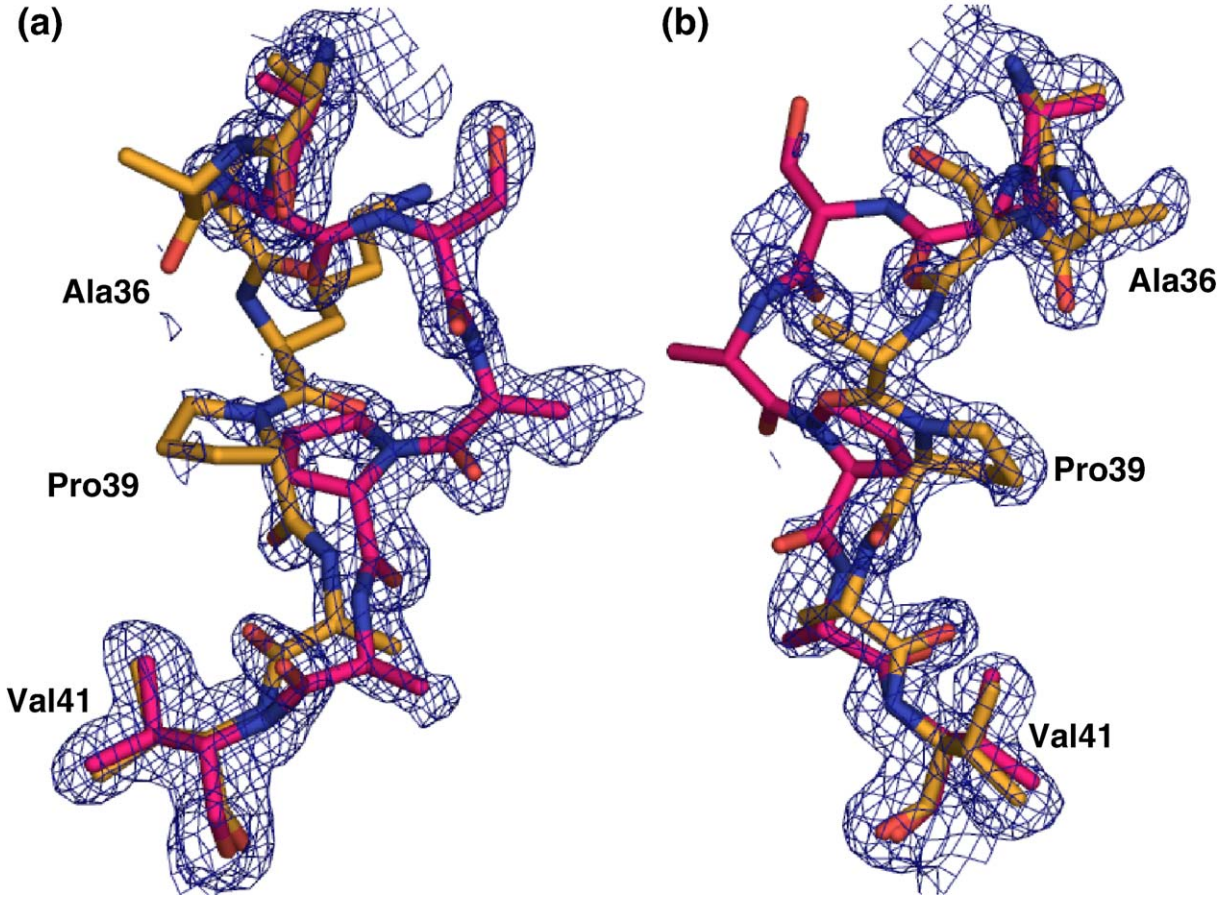

Figure 8. Omit electron density map of residues 35 to 41 of Mol B in (a) Xtal1 (hot pink), contoured at 2.2σ, with Xtal2 (orange) superimposed; and (b) Xtal2 (orange), contoured at 2.4σ, with Xtal1 (hot pink) superimposed. Maps are calculated by setting the occupancies of these residues equal to zero and calculating an omit electron density map using the CCP4 suite.

using SCALEPACK from the HKL package.[60] The complete diffraction data statistics are shown in Table 1.

Structure solution and refinement

All the structure determination and refinement calculations were performed using the CCP4 suite (Collaborative Computational Project, Number 4, 1994).[51]

Apo-WT

The structures of both Xtal1 and Xtal2 were determined using rigid body refinement in the CCP4 suite.[51] The coordinates of the apo-R111M structure (both of the molecules) were used as the original model. To generate an unbiased F_o-F_c map for the loop connecting the α2 to the βB in Mol B, residues 35–41 were deleted in Mol B of R111M. The F_o-F_c maps were calculated based on this unbiased model, which clearly showed that the loop connecting the α2 to the βB in Mol B is significantly different in the two structures of Xtal1 and Xtal2. In order to generate an unambiguous F_o-F_c electron density map of the deleted region, residues 35 to 41 of Mol B were built in each structure only after most of the water molecules and residues were built into the electron density and refined.

To confirm that we see two different conformations of the loop region in Mol B's of Xtal1 and Xtal2, the occupancies of residues in the loop region and neighboring residues before and after the loop (residues 35 to 41) were set to zero, 15 cycles of REFMAC refinement were run and an F_o-F_c electron density map was calculated using the CCP4 suite.[51] This is equivalent to deleting this region and is a REFMAC approach to calculating an omit map. The resulting F_o-F_c omit map for Xtal1 and Xtal2 clearly confirmed that region 36 to 40 in Mol B has two distinct conformations in these two crystals (Figure 8). Further, the two conformations of the loop were verified by calculating the simulated annealing-omit (sa-omit) map of this region using the CNS program.[61] The sa-omit map confirmed the two conformations for this loop. Interestingly both omit maps show some additional electron density for the other conformation of the loop in each structure, but the maps were not definitive enough to build an alternative conformation of the loop in each structure.

The model was visualized and manually rebuilt with the program TURBO-FRODO.[62] Version 5.2.0005 of REFMAC, the maximum-likelihood refinement program, was used to refine the structure against 90% of the data,[63] while 10% of data were chosen randomly for cross-validation, R_{free}.[64]

Ramachandran analysis of the structures calculated by program PROCHECK,[65] showed that in Xtal1 and Xtal2 94.3% and 93.5% of the residues are in the most favored region, respectively. In both structures the only residue in the disallowed region was Asp126 A, and the only residue in the generously allowed region was Asp126 B. These residues are located at the sharp turn of the βI–βJ hairpin loop and have higher than average *B*-factors and poor $2F_o$-F_c electron density maps. These two residues are reported to be in the same Ramachandran region in the CRABPII R111M structure and other retinoid-binding proteins.

F15W-CRABPII

The structure was determined as described for apo-WT CRABPII. Coordinates of both molecules of apo-WT CRABPII were used as the starting model.

CRABPII•RA

The structure was refined using the previously published structure of CRABPII•RA as a starting model.[44]

Protein Data Bank entry codes

The coordinates of each structure have been deposited in the PDB at Brookhaven with entry codes listed in Table 2.

Acknowledgements

We are grateful to beamline staff at BioCARS Sector 14, COM-CAT 32-ID and SBC-CAT 19-ID at the APS, Argonne National Laboratory. Use of the Advanced Photon Source was supported by the US Department of Energy, Office of Science, Office of Basic Energy Sciences, under contract no. W-31-109-ENG-38. Use of BioCARS Sector 14 was supported by the National Institutes of Health, National Center for Research Resources, under grant number RR07707. Particularly we thank BioCARS beamline scientist Dr V. Srajer. Use of the beamline 32-ID with beamline management and support provided by the IMCA-CAT staff at the Advanced Photon Source was supported by the companies of the Industrial Macromolecular Crystallography Association through a contract with the Center for Advanced Radiation Sources at the University of Chicago. Use of the Argonne National Laboratory Structural Biology Center beamlines at the Advanced Photon Source, was supported by the US Department of Energy, Office of Energy Research, under contract no. W-31-109-ENG-38. This research was supported by the NIH (GM84563 to J.H.G. and GM82800 to B.B.).

References

1. Giguere, V. (1994). Retinoic acid receptors and cellular retinoid-binding proteins–complex interplay in retinoid signaling. *Endocr. Rev.* **15**, 61–79.
2. DeLuca, L. M. (1991). Retinoids and their receptors in differentiation, embryogenesis, and neoplasia. *FASEB J.* **5**, 2924–2933.
3. Gudas, L. J., Sporn, M. B. & A. B., R. (1994). Cellular biology and biochemistry of the retinoids. In *The Retinoids: Biology, Chemistry, and Medicine* (Sporn, M. B., Roberts, A. B. & Goodman, D. S., eds), 2nd edit., pp. 443–520, Raven Press, New York.
4. Lotan, R. (1980). Effects of vitamin A and its analogs (retinoids) on normal and neoplastic cells. *Biochim. Biophys. Acta*, **605**, 33–91.
5. Chambon, P. (1996). A decade of molecular biology of retinoic acid receptors. *FASEB J.* **10**, 940–954.
6. Chomienne, C., Fenaux, P. & Degos, L. (1996). Retinoid differentiation therapy in promyelocytic leukemia. *FASEB J.* **10**, 1025–1030.
7. Delva, L., Bastie, J. N., Rochette-Egly, C., Kraiba, R., Balitrand, N., Despouy, G. *et al.* (1999). Physical and

functional interactions between cellular retinoic acid binding protein II and the retinoic acid-dependent nuclear complex. *Mol. Cell. Biol.* **19**, 7158–7167.
8. Tallman, M. S. (1996). Differentiating therapy in acute myeloid leukemia. *Leukemia*, **10**, 1262–1268.
9. Fisher, G. J. & Voorhees, J. J. (1996). Molecular mechanisms of retinoid actions in skin. *FASEB J.* **10**, 1002–1013.
10. Hong, W. K. & Itri, L. M. (1994). Retinoids and human cancer. In *The Retinoids: Biology, Chemistry, and Medicine* (Sporn, M. B., Roberts, A. B. & Goodman, D. S., eds), 2nd edit., pp. 597–630, Raven Press, New York.
11. Morrisskay, G. (1993). Retinoic acid and craniofacial development - molecules and morphogenesis. *Bioessays*, **15**, 9–15.
12. Mangelsdorf, D. J., Thummel, C., Beato, M., Herrlich, P., Schutz, G., Umesono, K. *et al.* (1995). The nuclear receptor superfamily—The 2nd decade. *Cell*, **83**, 835–839.
13. Leroy, P., Krust, A., Kastner, P., Mendelsohn, C., Zelent, A. & Chambon, P. (1992). Retinoic Acid Receptors. In *Retinoids in Normal Development and Teratogenesis* (Morriss-Kay, G., ed.), pp. 7–25, Oxford University Press, Oxford.
14. Leid, M., Kastner, P., Lyons, R., Nakshatri, H., Saunders, M., Zacharewski, T. *et al.* (1992). Purification, cloning, and Rxr identity of the Hela-Cell factor with which Rar or Tr Heterodimerizes to bind target sequences efficiently. *Cell*, **68**, 377–395.
15. Kreutz, M., Fritsche, J., Andreesen, R. & Krause, S. W. (1998). Regulation of cellular retinoic acid binding protein (CRABP II) during human monocyte differentiation in vitro. *Biochem. Biophys. Res. Commun.* **248**, 830–834.
16. Kliewer, S. A., Umesono, K., Mangelsdorf, D. J. & Evans, R. M. (1992). Retinoid X-receptor interacts with nuclear receptors in retinoic acid, thyroid-hormone and vitamin-D3 signaling. *Nature*, **355**, 446–449.
17. Sani, B. P. & Hill, D. L. (1974). Retinoic acid-binding-protein in chick-embryo metatarsal skin. *Biochem. Biophys. Res. Commun.* **61**, 1276–1282.
18. Ong, D. E. & Chytil, F. (1975). Retinoic acid-binding protein in rat tissue - partial-purification and comparison to rat tissue retinol-binding protein. *J. Biol. Chem.* **250**, 6113–6117.
19. Bailey, J. S. & Siu, C. H. (1988). Purification and partial characterization of a novel binding-protein for retinoic acid from neonatal rat. *J. Biol. Chem.* **263**, 9326–9332.
20. Ong, D. E., Newcomer, M. E. & Chytil, F. (1994). Cellular retinoid-binding proteins. In *The Retinoids: Biology, Chemistry, and Medicine* (Sporn, M. B., Roberts, A. B. & Goodman, D. S., eds), 2nd edit., pp. 283–318, Raven Press, New York.
21. Gaub, M. P., Lutz, Y., Ghyselinck, N. B., Scheuer, I., Pfister, V., Chambon, P. & Rochette-Egly, C. (1998). Nuclear detection of cellular retinoic acid binding proteins I and II with new antibodies. *J. Histochem. Cytochem.* **46**, 1103–1111.
22. Napoli, J. L. (1994). Retinoic acid homeostasis. Prespective roles of B-carotene, retinol, CRBP and CRABP. In *Vitamin A in Health and Disease* (Blomhoff, R., ed.), pp. 135–188, Marcel Dekker, New York.
23. Napoli, J. L. (1996). Retinoic acid biosynthesis and metabolism. *FASEB J.* **10**, 993–1001.
24. Napoli, J. L. (1999). Interactions of retinoid binding proteins and enzymes in retinoid metabolism. *Biochim. Biophys. Acta*, **1440**, 139–162.
25. Boylan, J. F. & Gudas, L. J. (1991). Overexpression of the cellular retinoic acid binding protein-I (Crabp-I) results in a reduction in differentiation-specific gene-expression in F9 teratocarcinoma cells. *J. Cell. Biol.* **112**, 965–979.
26. Boylan, J. F. & Gudas, L. J. (1992). The level of Crabp-I expression influences the amounts and types of all-trans-retinoic acid metabolites in F9 teratocarcinoma stem-cells. *J. Biol. Chem.* **267**, 21486–21491.
27. Dolle, P., Ruberte, E., Leroy, P., Morrisskay, G. & Chambon, P. (1990). Retinoic acid receptors and cellular retinoid binding-proteins. I. A systematic study of their differential pattern of transcription during mouse organogenesis. *Development*, **110**, 1133–1151.
28. Maden, M. (1994). Roles of retinoids in embryonic development. In *Vitamin A in Health and Disease* (Blomhoff, R., ed.), pp. 289–322, Marcel Dekker, New York.
29. Zheng, W. L., Bucco, R. A., Schmitt, M. C., Wardlaw, S. A. & Ong, D. E. (1996). Localization of cellular retinoic acid-binding protein (CRABP) II and CRABP in developing rat testis. *Endocrinology*, **137**, 5028–5035.
30. Ong, D. E. & Chytil, F. (1978). Cellular retinoic acid-binding protein from rat testis—purification and characterization. *J. Biol. Chem.* **253**, 4551–4554.
31. Wardlaw, S. A., Bucco, R. A., Zheng, W. L. & Ong, D. E. (1997). Variable expression of cellular retinol- and cellular retinoic acid-binding proteins in the rat uterus and ovary during the estrous cycle. *Biol. Reprod.* **56**, 125–132.
32. Zheng, W. L. & Ong, D. E. (1998). Spatial and temporal patterns of expression of cellular retinol-binding protein and cellular retinoic acid-binding proteins in rat uterus during early pregnancy. *Biol. Reprod.* **58**, 963–970.
33. Yamamoto, M., Drager, U. C., Ong, D. E. & McCaffery, P. (1998). Retinoid-binding proteins in the cerebellum and choroid plexus and their relationship to regionalized retinoic acid synthesis and degradation. *Eur. J. Biochem.* **257**, 344–350.
34. Banaszak, L., Winter, N., Xu, Z. H., Bernlohr, D. A., Cowan, S. & Jones, T. A. (1994). Lipid-binding proteins—a family of fatty-acid and retinoid transport proteins. *Adv. Protein Chem.* **45**, 89–151.
35. Budhu, A., Gillilan, R. & Noy, N. (2001). Localization of the RAR interaction domain of cellular retinoic acid binding protein-II. *J. Mol. Biol.* **305**, 939–949.
36. Budhu, A. S. & Noy, N. (2002). Direct channeling of retinoic acid between cellular retinoic acid-binding protein II and retinoic acid receptor sensitizes mammary carcinoma cells to retinoic acid-induced growth arrest. *Mol. Cell. Biol.* **22**, 2632–2641.
37. Jing, Y. K., Waxman, S. & Miray Lopez, R. (1997). The cellular retinoic acid binding protein II is a positive regulator of retinoic acid signaling in breast cancer cells. *Cancer Res.* **57**, 1668–1672.
38. Takase, S., Ong, D. E. & Chytil, F. (1986). Transfer of retinoic acid from its complex with cellular retinoic acid-binding protein to the nucleus. *Arch. Biochem. Biophys.* **247**, 328–334.
39. Dong, D., Ruuska, S. E., Levinthal, D. J. & Noy, N. (1999). Distinct roles for cellular retinoic acid-binding proteins I and II in regulating signaling by retinoic acid. *J. Biol. Chem.* **274**, 23695–23698.
40. Sessler, R. J. & Noy, N. (2005). A ligand-activated nuclear localization signal in cellular retinoic acid binding protein-II. *Mol. Cell.* **18**, 343–353.

41. Stryer, L. (1988). *Biochemistry*, 3rd edit., W.H. Freeman and Company, New York.
42. Cokol, M., Nair, R. & Rost, B. (2000). Finding nuclear localization signals. *EMBO Rep.* **1**, 411–415.
43. Chen, X., Tordova, M., Gilliland, G. L., Wang, L. C., Li, Y., Yan, H. G. & Ji, X. H. (1998). Crystal structure of apo-cellular retinoic acid-binding protein type II (R111M) suggests a mechanism of ligand entry. *J. Mol. Biol.* **278**, 641–653.
44. Kleywegt, G. J., Bergfors, T., Senn, H., Lemotte, P., Gsell, B., Shudo, K. & Jones, T. A. (1994). Crystal-structures of cellular retinoic acid-binding protein-I and protein-Ii in complex with all-*trans*-retinoic acid and a synthetic retinoid. *Structure*, **2**, 1241–1258.
45. Gunasekaran, K., Hagler, A. T. & Gierasch, L. M. (2004). Sequence and structural analysis of cellular retinoic acid-binding proteins reveals a network of conserved hydrophobic interactions. *Proteins: Struct. Funct. Genet.* **54**, 179–194.
46. Wang, L. C. & Yan, H. G. (1998). NMR study suggests a major role for Arg111 in maintaining the structure and dynamical properties of type II human cellular retinoic acid binding protein. *Biochemistry*, **37**, 13021–13032.
47. Wang, L. C., Li, Y. & Yan, H. G. (1997). Structure-function relationships of cellular retinoic acid-binding proteins—Quantitative analysis of the ligand binding properties of the wild-type proteins and site-directed mutants. *J. Biol. Chem.* **272**, 1541–1547.
48. Winter, N. S., Bratt, J. M. & Banaszak, L. J. (1993). Crystal-structures of holo and apo-cellular retinol-binding protein-Ii. *J. Mol. Biol.* **230**, 1247–1259.
49. Xu, Z. H., Bernlohr, D. A. & Banaszak, L. J. (1992). Crystal-structure of recombinant murine adipocyte lipid-binding protein. *Biochemistry*, **31**, 3484–3492.
50. Kabsch, W. & Sander, C. (1983). Dictionary of protein secondary structure-pattern-recognition of hydrogen-bonded and geometrical features. *Biopolymers*, **22**, 2577–2637.
51. Bailey, S. (1994). The Ccp4 suite - programs for protein crystallography. *Acta Crystallog. sect. D*, **50**, 760–763.
52. Crist, R. M., Vasileiou, C., Rabago-Smith, M., Geiger, J. H. & Borhan, B. (2006). Engineering a Rhodopsin protein surrogate. *J. Am. Chem. Soc.* **128**, 4522–4523.
53. Wang, L. C., Li, Y., Abildgaard, F., Markley, J. L. & Yan, H. G. (1998). NMR solution structure of type II human cellular retinoic acid binding protein: Implications for ligand binding. *Biochemistry*, **37**, 12727–12736.
54. Thompson, J. R., Bratt, J. M. & Banaszak, L. J. (1995). Crystal-structure of cellular retinoic acid-binding protein-I shows increased access to the binding cavity due to formation of an intermolecular beta-sheet. *J. Mol. Biol.* **252**, 433–446.
55. Haunerland, N. H., Jacobson, B. L., Wesenberg, G., Rayment, I. & Holden, H. M. (1994). 3-dimensional structure of the muscle fatty-acid-binding protein isolated from the desert locust Schistocerca-Gregaria. *Biochemistry*, **33**, 12378–12385.
56. Sacchettini, J. C., Gordon, J. I. & Banaszak, L. J. (1989). Refined apoprotein structure of rat intestinal fatty-acid binding-protein produced in Escherichia-Coli-(protein-structure x-ray crystallography fatty acid-protein interactions). *Proc. Natl Acad. Sci. USA*, **86**, 7736–7740.
57. Scapin, G., Gordon, J. I. & Sacchettini, J. C. (1992). Refinement of the structure of recombinant rat intestinal fatty acid-binding apoprotein at 1.2-Å resolution. *J. Biol. Chem.* **267**, 4253–4269.
58. Xu, Z. H., Bernlohr, D. A. & Banaszak, L. J. (1993). The adipocyte lipid-binding protein at 1.6-Å resolution-crystal-structures of the apoprotein and with bound saturated and unsaturated fatty-acids. *J. Biol. Chem.* **268**, 7874–7884.
59. Bergfors, T., Kleywegt, G. J. & Jones, T. A. (1994). Crystallization and preliminary-x-ray analysis of recombinant bovine cellular retinoic acid-binding protein. *Acta Crystallog. sect. D*, **50**, 370–374.
60. Otwinowski, Z. & Minor, W. (1997). Processing of X-ray diffraction data collected in oscillation mode. In *Methods in Enzymology* (Carter, C. W, Jr & Sweet, R. M., eds), vol. 276, pp. 307–326, Academic Press, New York.
61. Brunger, A. T., Adams, P. D., Clore, G. M., DeLano, W. L., Gros, P., Grosse-Kunstleve, R. W. *et al.* (1998). Crystallography and NMR system: A new software suite for macromolecular structure determination. *Acta Crystallog. sect. D*, **54**, 905–921.
62. Roussel, A. & Cambillau, C. (1989). Turbo-Frodo. In *Silicon Graphics Geometry Partners Directory*, Silicon Graphics, Mountain View.
63. Murshudov, G. N., Vagin, A. A. & Dodson, E. J. (1997). Refinement of macromolecular structures by the maximum-likelihood method. *Acta Crystallog. sect. D*, **53**, 240–255.
64. Brunger, A. T. (1993). Assessment of phase accuracy by cross validation—The Free R-Value-Methods and Applications. *Acta Crystallog. sect. D*, **49**, 24–36.
65. Laskowski, R. A., Macarthur, M. W., Moss, D. S. & Thornton, J. M. (1993). Procheck—A program to check the stereochemical quality of protein structures. *J. Appl. Crystallog.* **26**, 283–291.

Edited by R. Huber

(Received 11 May 2006; received in revised form 16 August 2006; accepted 22 August 2006)
Available online 26 August 2006